Radar reflectivity as a proxy for convective mass transport

G. L. Mullendore,[1] A. J. Homann,[1] K. Bevers,[2] C. Schumacher,[2]

G. L. Mullendore, Department of Atmospheric Sciences, University of North Dakota, 4149 University Avenue, Stop 9006, Grand Forks, ND 58202, USA. (gretchen@atmos.und.edu)

[1]Department of Atmospheric Sciences, University of North Dakota, Grand Forks, North Dakota

[2]Department of Atmospheric Sciences, Texas A&M University, College Station, Texas

Abstract. More observations of vertical mass transport in deep convection are needed to improve dynamical understanding of detrainment processes and for verification of transport models. A methodology for using radar reflectivity as a direct observation of vertical transport of mass from the boundary layer to the upper troposphere and lower stratosphere is investigated and the "level of maximum detrainment" (LMD) is proposed. The case investigated is the 26 January 1999 squall line from the TRMM-LBA field campaign. Echo-top heights and dual-Doppler derived divergence profiles are used to define the mass detrainment range. Over 10% of anvil echo tops occurred above the sounding-derived LNB of 15.4 km during the mature stage of the storm, and convective tops reached above 18 km. Anvil ice water content, with a simple correction for ice fall-speed, is found to be a good proxy for both the LMD, which for the storm analyzed is 11.25 km, and for the detrainment range of 6 to 17 km. More cases need to be analyzed to confirm the strength of this methodology, but the case study presented shows a strong correlation between anvil properties determined from radar reflectivity and the mass detrainment profile. Thus, radar reflectivity can be used as an indicator of the LMD to test model convective and transport parameterizations.

1. Introduction

Rapid vertical transport of chemical tracers from the boundary layer to the upper troposphere and lower stratosphere (UTLS) is accomplished primarily through convective transport in storms (e.g. Dickerson [1987]). In order for atmospheric chemical models to properly simulate the UTLS, the models first must properly simulate the level at which mass is detraining from deep convective updrafts. Better understanding of deep convective transport is important not only for chemical models, but also dynamical models, as updraft size and extent relates closely to the problem of heating profiles and water vapor transport, crucial for global momentum budgets and radiative budgets, as highlighted in recent studies (e.g. Schumacher et al. [2004]; Alexander et al. [2004]). Deep convective mass transport has been simulated (e.g. Stenchikov et al. [1996]; Mullendore et al. [2005]; Barth et al. [2007]; Charboureau et al. [2007]), but without more observations, results from cloud-resolving transport models remain relatively unconstrained.

The simplest way to estimate the level at which detrainment will occur is to calculate the level of neutral buoyancy (LNB) from a sounding using parcel theory. The radiosonde used, however, is often located a substantial distance in time or space from the immediate pre-storm environment, and therefore may have sampled an air mass very different from the air parcels being convected. Also, this parcel method of determining detrainment level is highly idealized, not accounting for the variability in initial parcel conditions or entrainment of environmental air along the upward trajectory of the surface parcel. The entrainment amounts and profiles can be approximated (e.g. Emanuel [1991]; Kain and Fritsch [1990]), but entrainment itself is highly variable, depending on factors such as the local environmental profile, storm classification and storm size (Cohen [2000]; Mullendore et al. [2005]).

Case studies have used chemical tracer retrievals from aircraft and sounding measurements to analyze observations of tracer transport in vigorous deep convection (e.g. Poulida et al. [1996]; Strom et al. [1999]; Hegglin et al. [2004]), but these observations are limited both spatially and temporally. Satellite observations have provided data over large areas on tracer plumes originating from deep convection (e.g. Ricaud et al. [2007]; Jiang et al. [2007]), but in a particular satellite observational data set, either the horizontal or vertical resolution of the measurements is coarse relative to the cloud-resolving regional models. Indirect methods, such as inferring deep convective transport based on the radiative balance in the upper troposphere [Folkins and Martin, 2005], also lack the resolution for cloud-resolving models.

To constrain cloud-resolving transport models, it is desirable to have a direct, cloud-scale measurement of the heights at which storm outflow *actually occurred*. Mullendore et al. [2005] found good agreement between the radar and model-simulated reflectivity in the forward anvil structure associated with a Severe Thunderstorm Electrification and Precipitation Study (STEPS) supercell (see their figure 14). The authors asserted that the reflectivity in the anvil region shows the transport of hydrometeors and serves as a proxy for tracer mass transport in deep convective updrafts. In this study, the goal is to expand on this assertion using reflectivity and dual-Doppler derived velocities from a squall line observed during the Tropical Rainfall Measuring Mission Large-Scale Biosphere-Atmosphere (TRMM-LBA) campaign.

The TRMM-LBA field experiment was conducted in Brazil in January and February of 1999 with the goals of learning more about tropical continental precipitation and validating TRMM satellite products [Silva Dias et al., 2002]. Cifelli et al. [2002] investigated the differences in various storm properties occurring in different meteorological regimes of TRMM-LBA, including storm morphology, rainfall amounts, and mass fluxes. This study expands upon the use of dual-Doppler derived velocities to estimate upward transport amounts integrated over the storm and proposes a methodology that could be used in the absence of dual-Doppler analysis. The term "level of maximum detrainment" (LMD) will be used to describe the level where maximum mass detrainment occurs. Cloud-top retrievals provide an upper bound on LMD and indicate the altitudes where troposphere-to-stratosphere exchange is most likely occurring, while reflectivity volumes illuminate the details of the vertical mass detrainment profile.

The current study builds on the dual-Doppler analysis done by Cifelli et al. [2002] by focusing on the deep convective mass transport, comparing the sounding-derived LNB to the LMD, and investigating the possibility of using anvil reflectivity retrievals as a proxy for convective mass transport. Section 2 gives a brief overview of the observations used. Section 3 describes the analyses performed and presents the echo-top and mass transport statistics. Summary and conclusions are presented in Section 4.

2. Observations

The observational platforms for TRMM-LBA included four radiosonde sites and two radars, the NASA TOGA C-band radar and the NCAR S-pol radar (figure 1). The dual-Doppler velocities are derived from the radial velocities observed by the NASA TOGA radar and the NCAR S-pol radar. The radar quality control and dual-Doppler processing was performed by researchers at Colorado State University [Cifelli et al., 2002; Lang and Rutledge , 2002]. Horizontal velocities (U and V) were corrected for precipitation fall speed by using a reflectivity-terminal fall velocity ($Z - V_t$) relationship. Vertical velocity was derived from the horizontal divergence calculations with downward integration using an exponential density profile. Note that although the horizontal divergence is available from the original dual-Doppler analysis, this study uses the derived vertical velocity data in order to look at upward-only velocities as well as calculate statistics on the vertical velocities.

The specific case being studied is the storm that moved westward through the TRMM-LBA observational domain on January 26th, 1999. The squall line formed at an outflow boundary from previous convection several hundred kilometers northeast of the TRMM-LBA sampling domain [Cifelli et al., 2002]. This storm was present in the region covered by the dual-Doppler lobes between 1950 and 2210 UTC and had a classic leading line-trailing stratiform structure [Houze, 1993]. The leading convective line and forward anvil were present in the dual-Doppler region between 1950 and 2030 UTC, which was the time period during which the storm was intensifying. The remaining times sampled primarily the stratiform region of the squall line.

3. Results

Due to its location in relation to the approaching squall line the 18 UTC sounding at Rebio-Jaru (figure 2, black line) was chosen as most representative of the pre-storm environment, and was used to estimate the LNB; both graphical and numerical methods of lifting a surface parcel returned a LNB altitude of 15.4 km. In contrast, the LNB calculated using the Abracos Hill sounding (figure 2, gray line) was 13.8 km. This high variability over a relatively small spatial area is due to the high variability in the boundary layer readings, highlighting the difficulty in relying on sounding data for storm characteristics.

3.1. Echo Top Retreivals

Following the methodology described in Steiner et al. [1995], the raining regions of the storm were classified as either convective or stratiform. The anvil was defined as the reflectivity observations with echo tops at or above 6 km with no reflectivity at 2.5 km following Frederick and Schumacher [2008].[1] The separation of the storm into convective and stratiform rain regions has a long tradition in the literature, but the anvil regions (i.e., horizontally homogeneous echo observed aloft but not reaching the ground) are often ignored or lumped in with the stratiform rain classification when analyzing reflectivity data. The anvil is, in fact, dynamically and radiatively distinct and is important for mass transport considerations. Note that often all cirrus is categorized as anvil; here the anvil is specifically the thick cirrus that is still attached to or recently produced by its convective source. For the specific squall line analyzed in this study, anvil region is the forward anvil and stratiform region is the trailing stratiform.

The storm was partitioned into three time periods; intensifying (1950-2030 UTC), mature (2040-2110 UTC), and dissipating (2120-2210 UTC). The echo tops, defined as the 0 dBZ line, for each region of the storm were then placed into altitude bins; the frequency of echo tops occurring at a given altitude and time is shown in figure 3. Echo tops were consistently produced in the region of the LNB (15.4 km) and although some of the observed tops may represent negatively buoyant air, some transport is expected to occur at all heights that hydrometeors penetrate, via turbulent mixing. In the intensifying stage of the storm, hydrometeors in the stratiform rain region are reaching above the LNB and strong convective updrafts at mid- to upper-levels are carrying hydrometeors to 18 km, indicating the possibility of mixing at high altitudes and transport directly into the tropical stratosphere. Echo tops for each storm region are highest in the mature stage of the storm, indicating stronger and more persistent updrafts. In the dissipating stage of the storm, vertical velocities are weaker and most hydrometeors are found below 16 km.

Mullendore et al. [2005] demonstrated that while turbulent processes do allow some parcels to achieve neutral buoyancy at high altitudes by mixing with stratospheric air, many parcels at cloud top in deep convective turrets are, in fact, negatively buoyant and will subsequently descend. In contrast, the anvil region, on convective time scales of an hour or two, is moving more horizontally than vertically and indicates a neutrally buoyant air mass. Interestingly, the echo tops of the anvil region remain high even in the later stage of the storm (figure 3c), showing that much of the anvil is generated by the deep cells during the mature stage of the storm and then remains aloft.

3.2. Mass Transport Profiles

While echo-top heights provide an upper bound of deep convective mass transport, echo-top data is insufficient to obtain a vertical profile and learn at what altitude the maximum detrainment is occurring. The final extent of the anvil associated with a particular storm depends on several factors not related to the strength and duration of the convective updrafts, including radiative interactions, upper level wind shear and magnitude, and upper level relative humidity. However, in an active storm, when time scales range from 30 minutes to several hours and spatial scales are on the order of the updraft width, the dominant factors in anvil production will be divergence in the updraft (strength of updraft) and upper level winds. While strong upper level winds can create some anvil from overshooting hydrometeors (Garrett et al. [2004]; Wang [2003]), the majority of anvil near the updraft will be due to vertical mass convergence. The extent and magnitude of the convergence, and likewise, the extent and concentration of hydrometeors in the anvil, describe the LMD.

3.2.1. Single Cross-Section

The convective line is redefined in this section as the region 25 km in width that is bounded on the west by the first reflectivity points that extend from 2 km to at least 8 km in altitude over a minimum of 5 km distance in the horizontal (figure 4a). This convective region definition differs from the traditional Steiner et al. [1995] reflectivity definition and from the methodology used in the previous section, and was chosen so that all regions of vertical mass convergence that may affect the forward anvil formation, including weaker dissipating cells, would be included. Note that although the stratiform region of the storm is responsible for some amount of mass transport, much of the transport occurring in the stratiform region is transport of recycled air that originated in the convective region [Gamache and Houze, 1983], or relatively small magnitude vertical transport of environmental air from the mid-troposphere [Gamache and Houze, 1982]; the likelihood of venting of boundary layer air with subsequent transport to high altitudes is unlikely in the stratiform region. Hence, this study focuses on the deep vertical transport in the convective regions of the storm. The possible role stratiform transport plays in the further lifting of air already processed by the deep convective updrafts will be investigated in a separate study. The convectively generated anvil is defined as in the previous section but constrained to be within 20 km of the convective line.

Figure 4c shows the mean vertical velocity (gray line) and mean reflectivity (black line) in the convective region of the cross-section shown. Values above 16 km are less representative of a mean value, as the number of echoes sharply decreases at that altitude. The velocity peaks at approximately 11 km, suggesting that the majority of parcels experience negative buoyancy above that height and hence begin to slow down. This slice was chosen for its well-developed anvil. The contour plot of the vertical velocity (panel b) suggests that the updraft sampled is dissipating, with a maturing cell that has moved farther back from the leading edge and is now elevated and cut-off from surface air.

Figure 4d shows the total divergence ($\frac{d\rho w}{dz}$, gray line) in the convective region and the total ice water mass (black line) in the anvil region of the cross-section. To calculate the vertical mass divergence, ρw is calculated at each velocity point (resolution is 0.5 km in the vertical and 1.0 km in the horizontal) by approximating $\rho(z)$ as $(\rho_0 exp^{z/H})$, where $\rho_0 = 1.22$ kg/m^3 and H = 7 km. Then a first order difference was used to calculate $\frac{d\rho w}{dz}$ along each column. To calculate the total vertical mass divergence profile, the divergence is integrated horizontally at each vertical level. The ice mass was estimated from reflectivity by assuming the majority of hydrometeors in the forward anvil are ice, then using equation 3 from Leary and Houze [1979]:

$$I = 8.0 \times 10^{-3} Z_I^{0.61}$$

where I is the ice water content (IWC), and Z_I is the reflectivity obtained after converting from the effective reflectivity by adding 6.7 dB. Note that although a range of magnitudes for IWC could be generated by choosing a different relation, the shape of the IWC profile would not change significantly.

The peak in negative vertical mass divergence indicates a peak in horizontal detrainment near 12 km, due to decreasing velocity in the updraft located about 50 km from SPOL (panel b). This primary peak in detrainment corresponds well with the peak in the total anvil ice water mass. A secondary peak in detrainment near 14 km corresponds to the elevated maximum located near 50 km from SPOL. As described above, the updraft sample is not at its most vigorous stage; the elevated maximum seen in the vertical velocity contours is partially responsible for the notch in divergence at 13 km. The notch is also partially caused by positive divergence of downdrafts in the volume. The notch is decreased in magnitude somewhat (i.e., convergence increases; figure 4d, dashed line) by calculating velocities from positive vertical velocities only (figure 4c, dashed line). As the goal is to capture detrainment primarily caused by the deep convective updrafts, only positive vertical velocities will be used to calculate deep convective transport in subsequent plots.

The correlation between vertical updraft mass convergence and anvil ice water mass supports the theory that anvil mass is a good proxy for convective detrainment level. However, not all cross-sections show such a strong relationship, as the updraft may be dissipated, or the updraft is strong but so young that the anvil has not yet had time to mature. To truly understand the overall correlation, a more statistical picture of the storm structure is needed.

3.2.2. Transport Statistics

To investigate the more general relationship between mass detrainment and anvil heights, contoured frequency by altitude diagrams (CFADs, Yuter and Houze [1995]) of the anvil and convective regions are calculated for multiple time steps (figure 5, panels a-d). The CFADs for reflectivity, vertical velocity, and vertical divergence ($\frac{d\rho w}{dz}$) in the convective line (figure 5, panels a-c) are constructed using 4 dBZ-sized bins centered from 2 dBZ to 58 dBZ, 2 m s^{-1}-sized bins centered from -20.5 m s^{-1} to 20.5 m s^{-1}, and 2x10^{-3} kg m^{-3} s^{-1}-sized bins centered from -0.02 to 0.02 kg m^{-3} s^{-1}, respectively. The CFAD for ice water content in the forward anvil (figure 5d) is constructed using 0.01 g m^{-3}-sized bins centered from 0.01 g m^{-3} to 0.2 g m^{-3}. The outermost bins extend to capture any values outside the range specified. The contours shown are 0.1, 1, 10, and 30% frequency. This analysis only includes times 1950 UTC to 2030 UTC, as afterwards, the leading convective line was no longer clearly defined.

Although we have used a different method to define the convective region, the CFADs of convective reflectivity and convective velocity, as well as the mean reflectivity (figure 5e) and mean vertical velocity (figure 5f), compare closely with the CFAD results shown in Cifelli et al. [2002] (see their figures 8 and 9). To determine the detrainment levels and the LMD, the vertical divergence in the convective region was calculated. The tilt in the 30% frequency contours (figure 5c) shows more vertical divergence, and horizontal entrainment, occurring at the low altitudes and more vertical convergence, and horizontal detrainment, occurring at the high altitudes. The profile of total divergence at each altitude (figure 5g) shows that there is net entrainment below 5 km and net detrainment between 5 km and 16.5 km. The altitude of maximum detrainment, as determined from maximum vertical convergence of positive vertical velocities, is 11.25 km. Panel h shows the anvil ice mass at each time snapshot, with the total anvil ice mass at time 2010 UTC in bold. Time 2010 UTC has the maximum ice mass as the forward anvil region within 20 km of the convective line starts leaving the domain at time 2020 UTC. The total ice water mass peaks at 10 km, with over 75% of the detrainment occurring at 2010 UTC between 7.5 and 13.0 km and over 50% between 8.5 and 11.5 km. The maximum in the ice water content at 10 km matches fairly well with the detrainment profile shown in panel g. However, ice is expected to fall as the anvil advects away from the source region of the updraft, necessitating a possible correction to the anvil altitudes.

3.2.3. Ice Fall Speed Adjustment

Assuming an ice fall speed of 0.3 m s^{-1} [Houze, 1993] and a mean outflow speed, we can introduce a correction to the anvil heights. The mean outflow speed is the speed the anvil is being transported westward in relation to the convective line. Over the analysis times, the average westward speed of the line is calculated to be 11 m s^{-1}, and the average dual-Doppler east-west velocity in the anvil is 16 m s^{-1} westward. Using the mean outflow speed of 5 m s^{-1}, the anvil would displace downwards 60 m for every 1 km in the horizontal it advects away from the convective line. Because the anvil has been constrained to the area within 20 km of the convective line, the maximum vertical adjustment is 1.2 km +/- 0.4 km (assuming 0.1 m s^{-1} uncertainty in the ice fall speed).

Figure 6a shows the new IWC CFAD and ice detrainment profile for time 2010 UTC using the fall speed adjustment. This adjustment has lifted the anvil estimated maximum detrainment level to 10.75 km (figure 6b), which compares well with the detrainment profile maximum of 11.25 km estimated from the total vertical divergence (shown again in figure 6c). For the case studied here, adjusted anvil location is a good proxy for mass detrainment profile.

The final LMD of approximately 11.25 km is 4 km below the Rebio-Jaru LNB of 15.4 km and 2.5 km below the LNB of 13.8 km from the Abracos Hill sounding. Simulations of this squall line are needed to investigate the mechanisms at work in more detail. The detrainment profile obtained from the analyses presented here will provide constraints on those future simulations.

4. Summary and Conclusions

The January 26th squall line from the TRMM-LBA field campaign is used as a test case for a methodology developed to use radar reflectivity as a direct observation of vertical transport of mass from the boundary layer to the upper troposphere and lower stratosphere. The "level of maximum detrainment" (LMD) is proposed to clarify the difference between the actual detrainment profile in deep convection and the level of neutral buoyancy (LNB) obtained from parcel theory.

Echo-top heights occur in a range containing the LNB, demonstrating the upper bound on convective transport and the altitudes at which turbulent mixing may cause irreversible transport. Over 10% of anvil echo tops occur above the LNB during the mature stage of the storm, and convective echo tops reach above 18 km. As some transport is expected at all heights that hydrometeors penetrate, this suggests some air is convectively transported directly into the stratosphere. By the dissipating stage of the storm, almost 10% of the anvil echo tops are still above the LNB. An algorithm for separating out the regions of cloud extent from Geostationary Operational Environmental Satellites (GOES) visible and infrared images that represent young, convectively-produced anvil based on TRMM radar observations is currently being investigated.

The reflectivity in the storm's forward anvil region is tested and found to be a good proxy for the LMD. The anvil region of interest is the anvil formed directly by convective turrets, in this storm defined as reflectivity retrievals with echo tops at or above 6 km with no reflectivity at 2.5 km that occur west (forward) and within 20 km of the convective line. A vertical profile of total anvil ice water mass is obtained by converting reflectivity to ice water mixing ratio and applying a simple ice fall-speed correction depending on horizontal distance from the convection. The resulting ice water mass profile correlates well with the LMD determined from the vertical velocity divergence profile. In the storm analyzed, the divergence-calculated LMD is at 11.25 km and estimated at 10.75 km using anvil reflectivity alone, with a detrainment range from 6 to 17 km, while the LNB, calculated with parcel theory, is calculated to be 15.4 km. More cases need to be analyzed to confirm the strength of this methodology, but this case study shows a strong correlation between anvil properties and the mass detrainment profile. Research is currently being conducted to determine how to best apply this methodology to different storm types (e.g. non-squall multicell storms, supercells). Also, tests are being conducted to use NEXRAD observations. Although some additional error will be introduced when storm-relative anvil speeds are not available, this methodology still shows promise for identifying the LMD. Radar reflectivity can be used as an indicator of the LMD to test model convective and transport parameterizations and also to constrain models that resolve convection.

Acknowledgments. The authors thank Timothy Lang, Robert Cifelli, Walter Petersen and Steven Rutledge of Colorado State University, and Lawrence Carey of University of Alabama, Huntsville for use of the processed radar data from TRMM-LBA. The authors also thank Mary Barth and the anonymous reviewers for valuable feedback. This work was completed with support from ND EPSCoR New Faculty Startup project number 43700−2210−UND0013943.

Notes

1. The gridded reflectivity field contained poorly resolved features in the most northern 20 km of the domain and most eastern 5 km, so these regions were excluded from the analyses.

References

Alexander, M. J., P. T. May and J. H. Beres, 2004: Gravity waves generated by convection in the Darwin area during the Darwin Area Wave Experiment. *Journal of Geophysical Research*, **109**(D20S04), doi:10.1029/2004JD004729.

Barth, M. C., S.-W. Kim, C. Wang, K. E. Pickering, L. E. Ott, G. Stenchikov, M. Leriche, S. Cautenet, J.-P. Pinty, C. Barthe, C. Mari, J. H. Helsdon, R. D. Farley, A. M. Fridlind, A. S. Ackerman, V. Spiridonov and B. Telenta, 2007: Cloud-scale model intercomparison of chemical constituent transport in deep convection. *Atmospheric Chemistry and Physics*, **7**(18), 4709–4731.

Chaboureau, J.-P., J.-P. Cammas, J. Duron, P. J. Mascart, N. M. Sitnikov, and H.-J. Voessing, 2007: A numerical study of tropical cross-tropopause transport by convective overshoots. *Atmospheric Chemistry and Physics*, **7**, 1731–1740.

Cifelli, R., W. A. Petersen, L. D. Carey and S. A. Rutledge, 2002: Radar observations of the kinematic, microphysical and precipitation characteristics of two MCSs in TRMM LBA. *Journal of Geophysical Research*, **107**(D20), doi:10.1029/2000JD000264.

Cohen, C., 2000: A quantitative investigation of entrainment and detrainment in numerically simulated cumulonimbus clouds. *Journal of the Atmospheric Sciences*, **57**(10), 1657–1674.

Dickerson, R. R., 1987: Thunderstorms: An important mechanism in the transport of air pollutants. *Science*, **235**, 460–465.

Emanuel, K. A., 1991: A scheme for representing cumulus convection in large-scale models. *Journal of the Atmospheric Sciences*, **48**(21), 2313–2335.

Folkins, I. and R. V. Martin, 2005: The vertical structure of tropical convection and its impact on the budgets of water vapor and ozone. *Journal of the Atmospheric Sciences*, **62**, 1560–1573.

Frederick, K. and C. Schumacher, 2008: Anvil characteristics as seen by c-pol during the tropical warm pool international cloud experiment (twp-ice). *Monthly Weather Review*, **136**(1), 206–222.

Gamache, J. F. and R. A. Houze, 1982: Mesoscale air motions associated with a tropical squall line. *Monthly Weather Review*, **110**(2), 118–135.

Gamache, J. F. and R. A. Houze, 1983: Water budget of a mesoscale convective system in the tropics. *Journal of the Atmospheric Sciences*, **40**(7), 1835–1850.

Garrett, T. J., A. J. Heymsfield, M. J. McGill, B. A. Ridley, D. G. Baumgardner, T. P. Bui and C. R. Webster, 2004: Convective generation of cirrus near the tropopause. *Journal of Geophysical Research*, **109**(D21203), doi:10.1029/2004JD004952.

Hegglin, M. I., D. Brunner, H. Wernli, C. Schwierz, O. Martius, P. Hoor, H. Fischer, N. Spelten, C. Schiller, M. Krebsbach, U. Parchatka, U. Weers, J. Staehelin and T. Peter, 2004: Tracing troposphere-to-stratosphere transport above a mid-latitude deep convective system. *Atmospheric Chemistry and Physics Discussions*, **4**, 169–206.

Houze, Jr., R. A., 1993: *Cloud Dynamics*. Academic Press.

Jiang, J. H., N. J. Livesey, H. Su, L. Neary, J. C. McConnell and N. A. D. Richards, 2007: Connecting surface emissions, convective uplifting, and long-range transport of carbon monoxide in the upper troposphere: New observations from the aura microwave limb sounder. *Geophys. Res. Lett.*, **34**(L18812), doi:10.1029/2007GL030638.

Kain, J. S. and J. M. Fritsch, 1990: A one-dimensional entraining/detraining plume model and its application in convective parameterization. *Journal of the Atmospheric Sciences*, **47**(23), 2784–2802.

Lang, T. J. and S. A. Rutledge, 2002: Relationships between convective storm kinematics, precipitation, and lightning. *Monthly Weather Review*, **130**, 2492–2506.

Leary, C. A. and R. A. Houze, 1979: Melting and evaporation of hydrometeors in precipitation from the anvil clouds of deep tropical convection. *Journal of the Atmospheric Sciences*, **36**(4), 669–679.

Mullendore, G. L., D. R. Durran and J. R. Holton, 2005: Cross-tropopause tracer transport in midlatitude convection. *J. Geophys. Res.*, **110**(D06113), doi:10.1029/2004JD005059.

Poulida, O., R. R. Dickerson and A. Heymsfield, 1996: Stratosphere-troposphere exhange in a midlatitude mesoscale convective complex 1. Observations. *Journal of Geophysical Research*, **101**, 6823–6839.

Ricaud, P., B. Barret, J.-L. Attié, E. Motte, E. Le Flochmoën, H. Teyssèdre, V.-H. Peuch, N. Livesey, A. Lambert and J.-P. Pommereau, 2007: Impact of land convection on troposphere-stratosphere exchange in the tropics. *Atmospheric Chemistry and Physics*, **7**(21), 5639–5657.

Schumacher, C., R. A. Houze, Jr and I. Kraucunas, 2004: The tropical dynamical response to latent heating estimates derived from the TRMM precipitation radar. *Journal of the Atmospheric Sciences*, **61**, 1341–1358.

Silva Dias, M. A. F., and Coauthors, 2002: Cloud and rain processes in a biosphere-atmosphere interaction context in the Amazon Region. *Journal of Geophysical Research*, **107**, 8072, doi:10.1029/2001JD000335.

Steiner, M., R. A. Houze, Jr and S. E. Yuter, 1995: Climatological characterization of three-dimensional storm structure from operational radar and rain gauge data. *Journal of Applied Meteorology*, **34**, 1978–2007.

Stenchikov, G., R. Dickerson, K. Pickering, W. Ellis, B. Doddridge, S. Kondragunta, O. Poulida, J. Scala and W. Tao, 1996: Stratosphere-troposphere exchange in a midlatitude mesoscale convective complex 2. Numerical simlulations. *Journal of Geophysical Research*, **101**, 6837–6851.

Strom, J., H. Fischer, J. Lelieveld and F. Schroder, 1999: In situ measurements of microphysical properties and tracer gases in two cumulonimbus anvils over western Europe. *Journal of Geophysical Research*, **104**, 12221–12226.

Wang, P. K., 2003: Moisture plumes above thunderstorm anvils and their contributions to cross-tropopause transport of water vapor in midlatitudes. *Journal of Geophysical Research*, **108**, 4194,doi:10.1029/2002JD002581.

Yuter, S. E. and R. A. Houze, 1995: Three-dimensional kinematic and microphysical evolution of florida cumulonimbus. part iii: Vertical mass transport, maw divergence, and synthesis. *Monthly Weather Review*, **123**(7), 1964–1983.

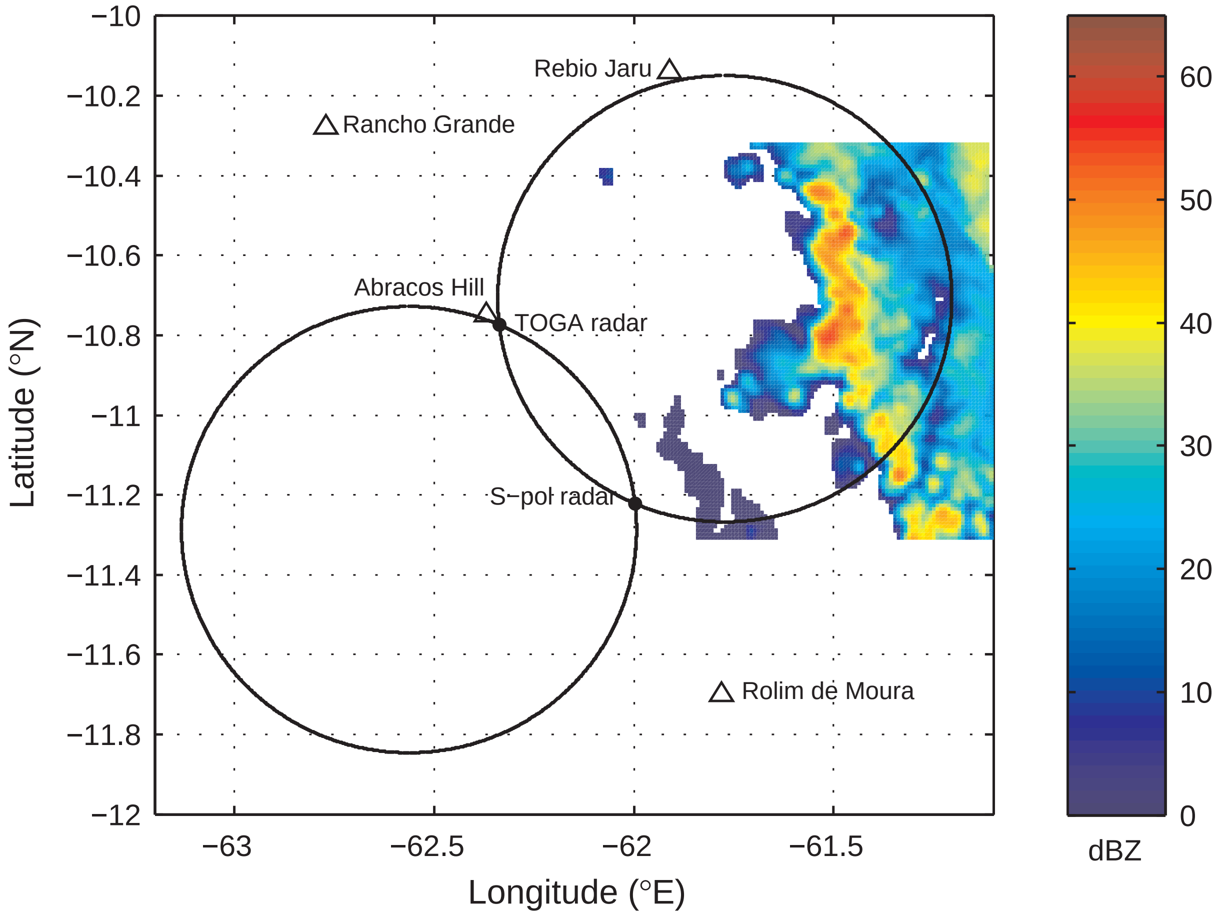

Figure 1. The TRMM-LBA sounding (triangles) and radar platforms (filled circles) used in this study. The dual-Doppler lobes are shown as open circles. Reflectivity is shown for altitude of 5 km at time 1950 UTC.

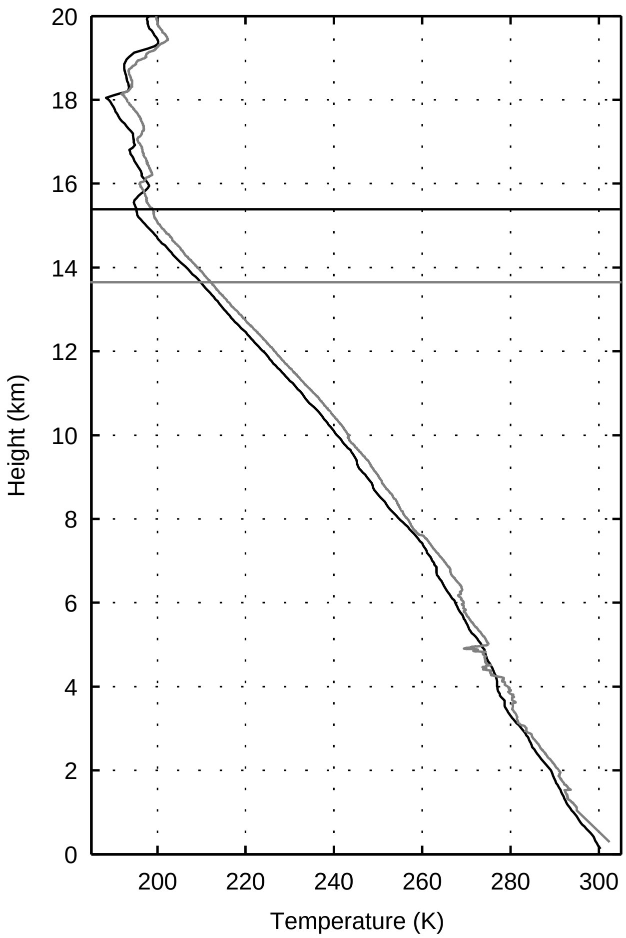

Figure 2. Temperature profiles and LNB altitudes (horizontal lines) for the January 26, 1999, 18 UTC soundings from Rebio-Jaru (black) and Abracos Hill (gray).

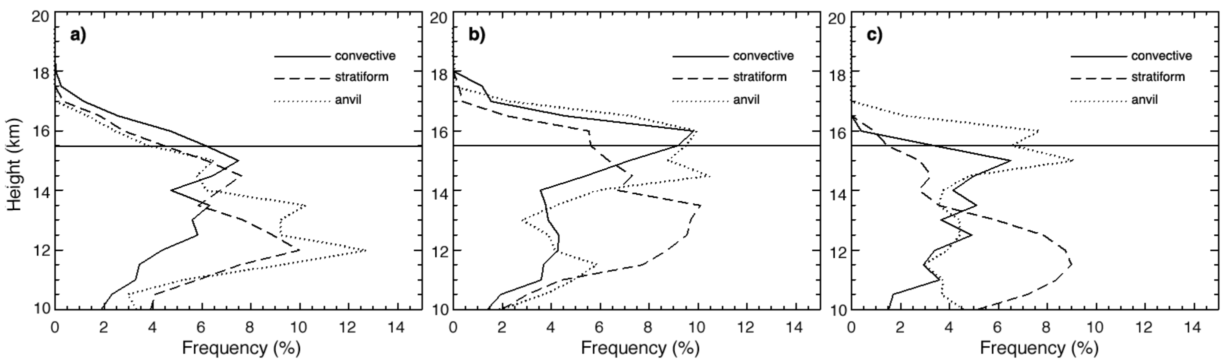

Figure 3. Reflectivity echo tops from the a) intensifying, b) mature, and c) dissipating stages of the January 26th squall line. Frequency of occurrence of echo top at each altitude is shown for convective (solid line), stratiform (dashed line), and anvil (dotted line) regions of the storm. The LNB is shown as a horizontal solid line.

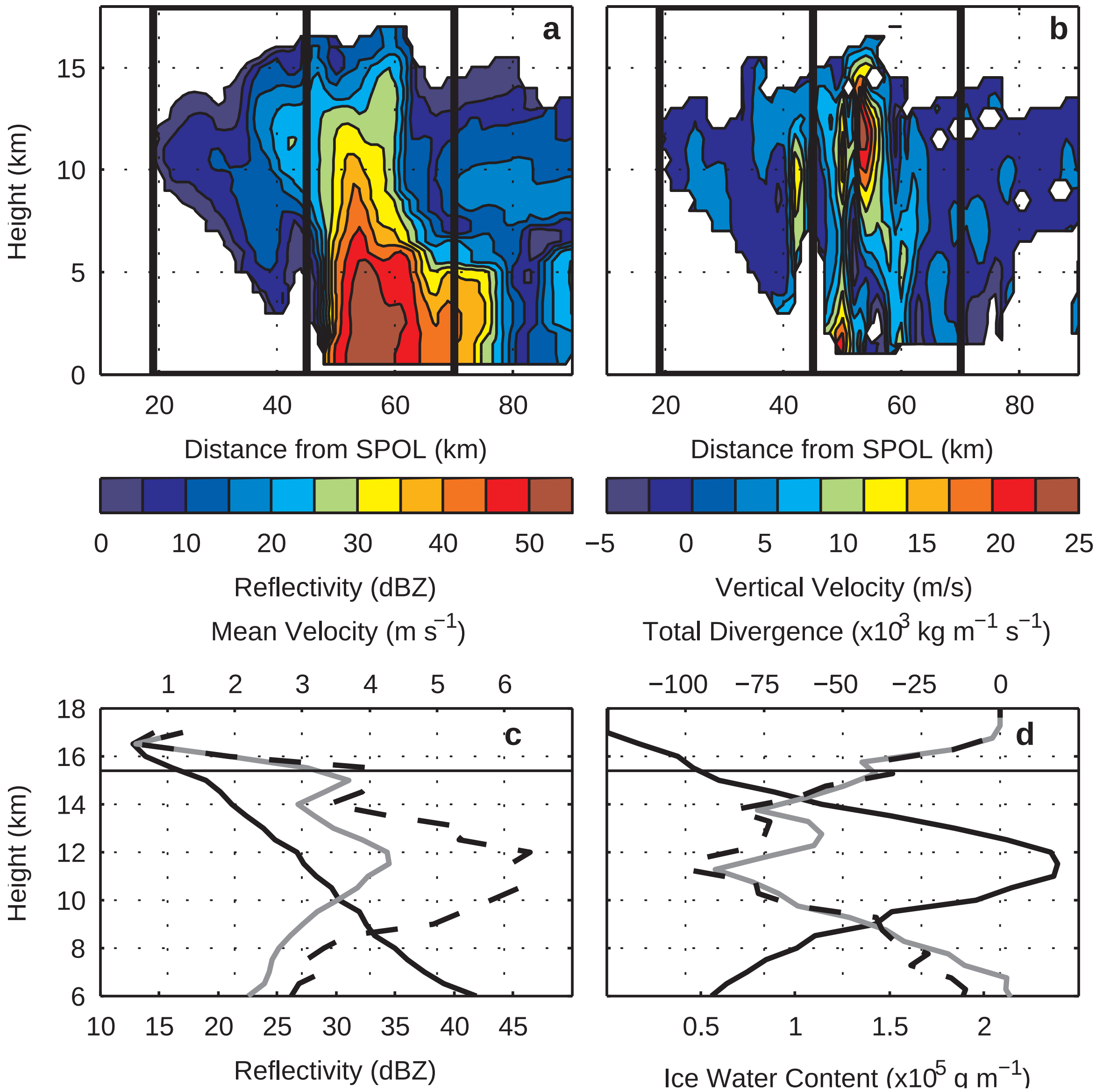

Figure 4. (a, b) Vertical cross-section taken perpendicular to line at 1950 UTC, showing reflectivity (a) and vertical velocity (b) in x and z, with the anvil and convective regions shown as boxes. The dual-Doppler domain extends an additional 60 km to the west. (c) Mean vertical velocity (gray line), mean vertical positive velocity (dashed line) and mean reflectivity (black line) in the convective region of the cross-section. (d) Total divergence ($\frac{d\rho w}{dz}$, gray line) and total divergence of positive velocities (dashed line) in the convective region and the total ice water mass (black line) in the anvil region of the cross-section. Horizontal line shows Rebio-Jaru LNB.

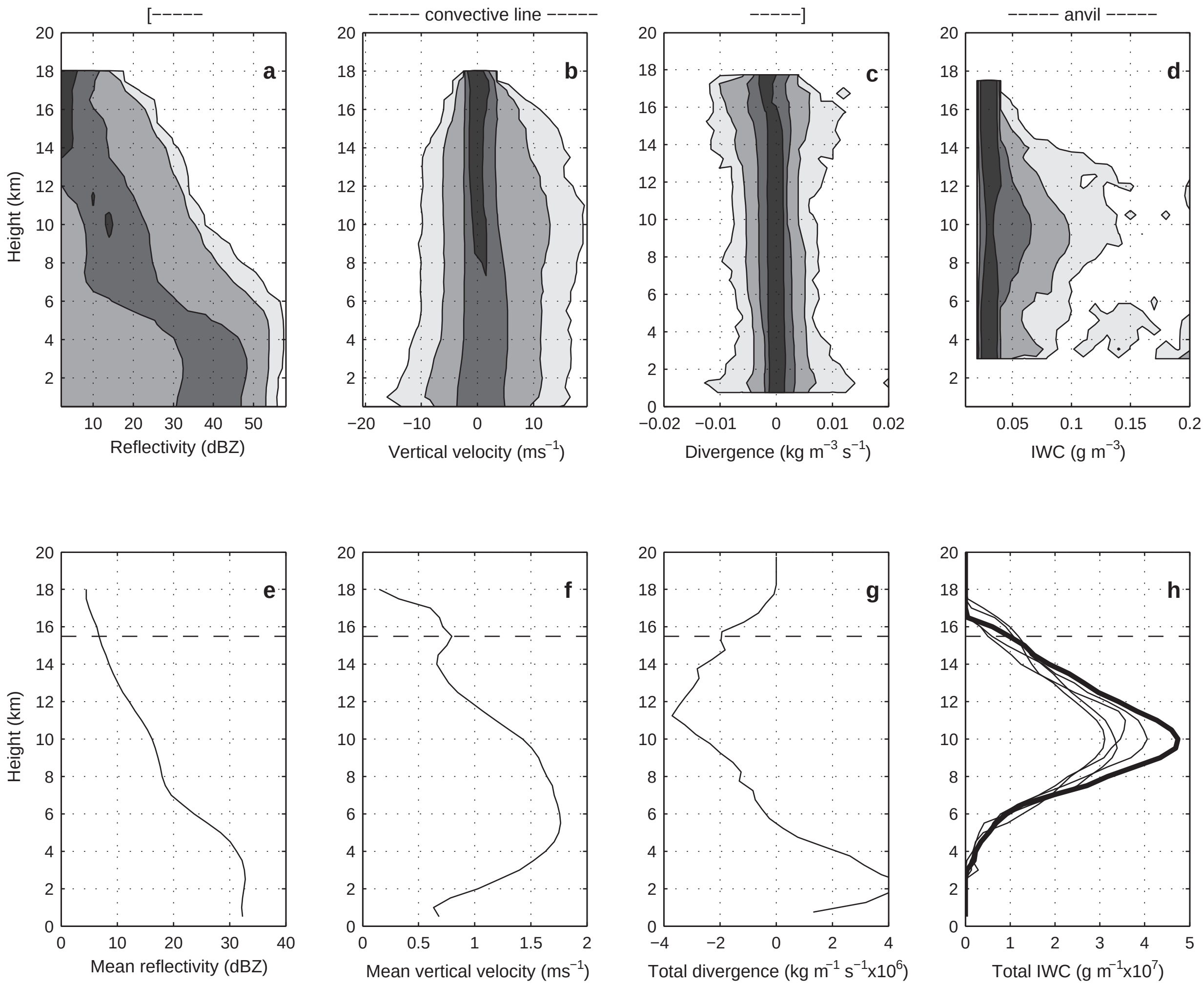

Figure 5. Analysis of times 1950 UTC to 2030 UTC in the Jan. 26 squall line. Panels a-c: Contoured frequency by altitude diagrams (CFADs) of a) reflectivity, b) vertical velocity, and c) vertical divergence in the convective line. Panel d: CFAD of ice water content in the forward anvil. Contours shown are 0.1, 1, 10, and 30% frequency. See text for details on bins chosen. Panels e-f: Mean e) reflectivity and f) vertical velocity for the convective line region at each altitude. Panel g: Total vertical divergence in convective line at each altitude. Panel h: Total ice water mass in forward anvil at each altitude, at each time slice. The anvil at 2010 UTC is shown as a thick solid line. In all bottom panels, the LNB is shown as a horizontal dashed line.

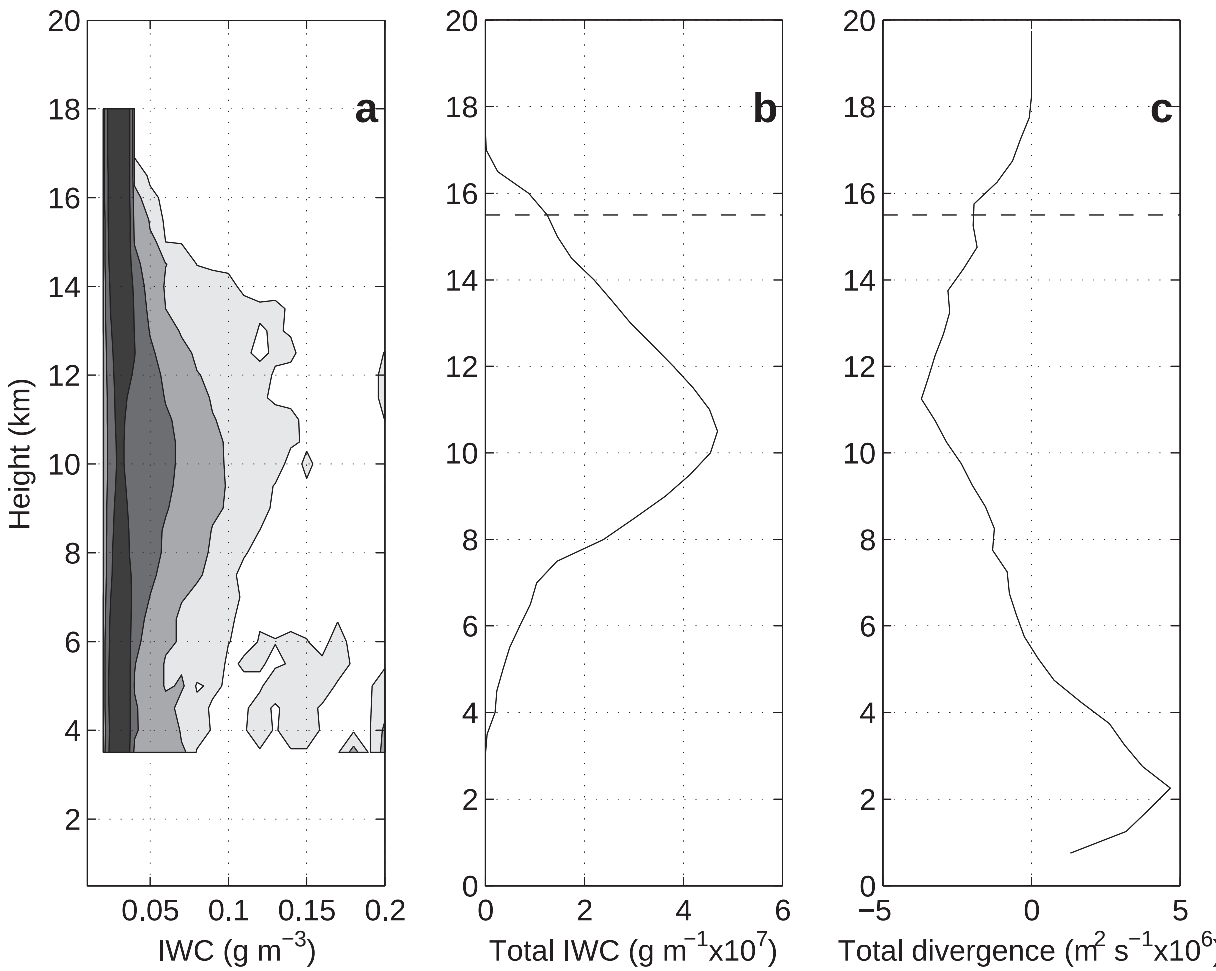

Figure 6. a) CFAD of ice water content from 1950-2030 UTC and b) total ice water mass at 2010 UTC for anvil profiles adjusted by ice fall speed. c) Total vertical divergence for positive vertical velocities. LNB shown as dashed horizontal line in panels b and c.